Supporting Information for

Folding a single high-genus surface into a repertoire of metamaterial functionalities

Xiangxin Dang, Stefano Gonella and Glaucio H. Paulino

Stefano Gonella, Glaucio H. Paulino.
E-mail: sgonella@umn.edu, gpaulino@princeton.edu

This PDF file includes:

Other supporting materials for this manuscript include the following:

Movies S1 to S5

Supporting Information Text

1. Dihedral angle relationships

In this section, we derive the relationships between the dihedral angles around one node of the folded-kirigami unit cell. We consider the equilateral-triangular unit cell in Fig. S1*A*. To simplify the formulation, we apply 3-fold rotational symmetry so that the folding process involves one degree of freedom. Consequently, we have three dependent dihedral angles: the angle θ between the base and a wing, the angle ξ between a wing and a flap, and the angle φ between two flaps. We draw an auxiliary sphere centered at the node. The sphere intersects with the unit cell, forming a spherical 5-gon (the blue curves in Fig. S1*A*). The sector angle α is the interior angle of the base equilateral triangle; β is the interior angle of a flap; and the interior angle of a wing is $\pi/2$. The magenta spherical triangle (of side lengths $\tilde{\beta}$, $\tilde{\beta}$, and γ) is constructed by extending the two sides of length $\pi/2$ and closing the third side with the geodesic line. The dihedral angles are illustrated in Fig. S1*B*, including θ, ξ, and φ and more that we need in the following formulation. First, we apply spherical cosine rules to the spherical triangle of side lengths α, $\tilde{\beta}+\pi/2$, and $\tilde{\beta}+\pi/2$:

$$\cos\left(\tilde{\beta}+\frac{\pi}{2}\right)=\cos\alpha\left[\cos\left(\tilde{\beta}+\frac{\pi}{2}\right)\right]+\sin\alpha\left[\sin\left(\tilde{\beta}+\frac{\pi}{2}\right)\right]\cos\theta, \quad [1]$$

$$\cos\alpha=\left[\cos\left(\tilde{\beta}+\frac{\pi}{2}\right)\right]^2+\left[\sin\left(\tilde{\beta}+\frac{\pi}{2}\right)\right]^2\cos\tilde{\varphi}. \quad [2]$$

Equation (1) leads to

$$\tilde{\beta}=-\arctan\left(\cot\frac{\alpha}{2}\cos\theta\right). \quad [3]$$

Equations (2) and (3) lead to

$$\tilde{\varphi}=2\arccos\left(\cos\frac{\alpha}{2}\sin\theta\right). \quad [4]$$

Then, we apply spherical cosine rules to the spherical triangle of side lengths γ, $\tilde{\beta}$, and $\tilde{\beta}$:

$$\cos\gamma=(\cos\tilde{\beta})^2+(\sin\tilde{\beta})^2\cos\tilde{\varphi}, \quad [5]$$

and to the spherical triangle of side lengths γ, β, and β:

$$\cos\gamma=(\cos\beta)^2+(\sin\beta)^2\cos\varphi. \quad [6]$$

Equations (3)–(5) lead to

$$\boxed{\gamma=-2\arcsin\left(\cos\frac{\alpha}{2}\cos\theta\right)}. \quad [7]$$

Notice that we have the relationship

$$\beta=\frac{\pi-\alpha}{2}. \quad [8]$$

Equations (6)–(8) lead to

$$\boxed{\varphi=2\theta-\pi}. \quad [9]$$

Again, we apply spherical cosine rules to the spherical triangle of side lengths γ, β, and β:

$$\cos\beta=\cos\beta\cos\gamma+\sin\beta\sin\gamma\cos\eta, \quad [10]$$

and to the spherical triangle of side lengths γ, $\tilde{\beta}$, and $\tilde{\beta}$:

$$\cos\tilde{\beta}=\cos\tilde{\beta}\cos\gamma+\sin\tilde{\beta}\sin\gamma\cos\tilde{\eta}. \quad [11]$$

Equations (8) and (10) lead to

$$\eta=\arccos\left(\tan\frac{\alpha}{2}\tan\frac{\gamma}{2}\right). \quad [12]$$

Equations (3), (7), and (11) lead to

$$\tilde{\eta}=\arccos\left(-\frac{\sin\alpha\cos\theta}{\sin\gamma}\right). \quad [13]$$

Notice that we have the relationship

$$\xi=\pi-(\eta-\tilde{\eta}). \quad [14]$$

Finally, Eqs. (12)–(14) lead to

$$\boxed{\xi=\pi-\arccos\left(\tan\frac{\alpha}{2}\tan\frac{\gamma}{2}\right)+\arccos\left(-\frac{\sin\alpha\cos\theta}{\sin\gamma}\right)}. \quad [15]$$

According to Eqs. (7), (9), and (15), we know that the dihedral angles φ and ξ are dependent on the dihedral angle θ. In the above derivation, we only use the local information—side lengths and angles meeting at the specific node, including the local interior angle of the base triangle $\alpha=\pi/3$. The global shape of the base triangle does not affect the results. Therefore, the formulation can be directly applied to the square unit cell by simply setting $\alpha=\pi/2$ (Fig. S1*C*), or to general irregular convex polygons with the corresponding value of α.

2. Formulation on kagome folded kirigami

In this section, we formulate node positions on the crease-slit patterns of the kagome folded kirigami. Specifically, we consider the kagome kirigami with two repeating constituent triangles (Fig. S2*A*, *Left*). Consistent with the kagome kirigami pattern, the crease-slit pattern of the folded kirigami is also composed of two repeating patches (Fig. S2*A*, *Right*). We denote the side lengths of the two triangles by a_i, b_i, and c_i for $i = 1$ and 2. Then, the interior angles α_i, β_i, and γ_i can be calculated by the cosine rules:

$$\begin{aligned} \alpha_i &= \frac{a_i^2 + c_i^2 - b_i^2}{2a_i c_i}, \\ \beta_i &= \frac{a_i^2 + b_i^2 - c_i^2}{2a_i b_i}, \\ \gamma_i &= \frac{b_i^2 + c_i^2 - a_i^2}{2b_i c_i}, \end{aligned} \tag{16}$$

for $i = 1$ and 2. On the kagome kirigami pattern, we denote the twist angles between one triangle and its three neighbors by θ, ξ, and η (Fig. S2*B*). Considering the translation symmetry of the kirigami pattern, the three twist angles are dependent on each other:

$$\boxed{\begin{aligned} \xi &= \alpha_1 - \beta_2 + \theta, \\ \eta &= \alpha_2 - \gamma_1 + \theta. \end{aligned}} \tag{17}$$

On the crease-slit pattern of the folded kirigami, the twist angles are equally distributed to the adjacent patches (Fig. S2*B*). To formulate the node positions on the repeating patches, we build up local coordinate systems as shown in Fig. S2*C*. Our goal is to give position vectors of all the nodes A_i, B_i, C_i, A_{ij}, B_{ij}, and C_{ij} for $i = 1$ and 2, and $j = 1, 2, ..., 6$, such that the whole crease-slit pattern can be easily obtained by translating the repeating patches. Recall that, for given base triangles, the node positions are dependent on two parameters—width of the rectangular wings h and residual side length of the truncated flaps s (see Fig. S1*A* for the wings and flaps). Since the flaps are meant to be folded and attached to the wings for the folded kirigami, the residual side length s should not be larger than the lengths of the wings (i.e., $a_i,\ b_i,\ c_i$). Moreover, the residual side length s should not be larger than the length of any flap before truncation (i.e., $h/\tan(\alpha_i/2),\ h/\tan(\beta_i/2),\ h/\tan(\gamma_i/2)$). Altogether, we have the following constraint:

$$\boxed{s \le \min\left\{ a_i,\ b_i,\ c_i,\ \frac{h}{\tan(\alpha_i/2)},\ \frac{h}{\tan(\beta_i/2)},\ \frac{h}{\tan(\gamma_i/2)} \;\middle|\; i = 1, 2 \right\}.} \tag{18}$$

In practice, we can specify s by its maximum value to make the truncated flaps as large as possible, such that the folding and attaching process can be easier. We denote the common edge lengths of adjacent flaps by p_i, q_i and r_i, which can be calculated by

$$\begin{aligned} p_i &= \frac{s}{\sin(\pi/2 - \alpha_i/2)}, \\ q_i &= \frac{s}{\sin(\pi/2 - \beta_i/2)}, \\ r_i &= \frac{s}{\sin(\pi/2 - \gamma_i/2)}, \end{aligned} \tag{19}$$

for $i = 1$ and 2. We denote the normal vectors of the base triangle edges by $\mathbf{l}_i, \mathbf{m}_i$, and $\mathbf{n}_i$, which can be expressed as

$$\begin{aligned} \mathbf{l}_i &= (0,\ -1), \\ \mathbf{m}_i &= (\sin\beta_i,\ \cos\beta_i), \\ \mathbf{n}_i &= (-\sin\alpha_i,\ \cos\alpha_i), \end{aligned} \tag{20}$$

for $i = 1$ and 2. The node positions on the base triangles are given by

$$\begin{aligned} \overrightarrow{A_i} &= (0,\ 0), \\ \overrightarrow{B_i} &= (a_i,\ 0), \\ \overrightarrow{C_i} &= (c_i\cos\alpha_i,\ c_i\sin\alpha_i), \end{aligned} \tag{21}$$

for $i = 1$ and 2. Finally, we can write the rest of the position vectors:

$$
\begin{aligned}
\overrightarrow{A_{i1}} &= \overrightarrow{A_i} + h\mathbf{n}_i, \\
\overrightarrow{A_{i2}} &= \overrightarrow{A_i} + h\mathbf{l}_i, \\
\overrightarrow{A_{i3}} &= \begin{cases} \overrightarrow{A_{i1}} + \left(s\tan\dfrac{\theta}{2}\right)\mathbf{n}_i, \ i = 1, \\ \overrightarrow{A_{i2}} + \left(s\tan\dfrac{\theta}{2}\right)\mathbf{l}_i, \ i = 2, \end{cases} \\
\overrightarrow{A_{i4}} &= \overrightarrow{A_{i1}} - \frac{s}{c_i}\left(\overrightarrow{C_i} - \overrightarrow{A_i}\right), \\
\overrightarrow{A_{i5}} &= \overrightarrow{A_{i1}} + p_i \frac{\overrightarrow{A_{i1}} + \overrightarrow{A_{i2}} - 2\overrightarrow{A_i}}{\|\overrightarrow{A_{i1}} + \overrightarrow{A_{i2}} - 2\overrightarrow{A_i}\|}, \\
\overrightarrow{A_{i6}} &= \overrightarrow{A_{i2}} - \frac{s}{a_i}\left(\overrightarrow{B_i} - \overrightarrow{A_i}\right),
\end{aligned}
\tag{22}
$$

$$
\begin{aligned}
\overrightarrow{B_{i1}} &= \overrightarrow{B_i} + h\mathbf{l}_i, \\
\overrightarrow{B_{i2}} &= \overrightarrow{B_i} + h\mathbf{m}_i, \\
\overrightarrow{B_{i3}} &= \begin{cases} \overrightarrow{B_{i1}} + \left(s\tan\dfrac{\xi}{2}\right)\mathbf{l}_i, \ i = 1, \\ \overrightarrow{B_{i2}} + \left(s\tan\dfrac{\xi}{2}\right)\mathbf{m}_i, \ i = 2, \end{cases} \\
\overrightarrow{B_{i4}} &= \overrightarrow{B_{i1}} - \frac{s}{a_i}\left(\overrightarrow{A_i} - \overrightarrow{B_i}\right), \\
\overrightarrow{B_{i5}} &= \overrightarrow{B_{i1}} + q_i \frac{\overrightarrow{B_{i1}} + \overrightarrow{B_{i2}} - 2\overrightarrow{B_i}}{\|\overrightarrow{B_{i1}} + \overrightarrow{B_{i2}} - 2\overrightarrow{B_i}\|}, \\
\overrightarrow{B_{i6}} &= \overrightarrow{B_{i2}} - \frac{s}{b_i}\left(\overrightarrow{C_i} - \overrightarrow{B_i}\right),
\end{aligned}
\tag{23}
$$

$$
\begin{aligned}
\overrightarrow{C_{i1}} &= \overrightarrow{C_i} + h\mathbf{m}_i, \\
\overrightarrow{C_{i2}} &= \overrightarrow{C_i} + h\mathbf{n}_i, \\
\overrightarrow{C_{i3}} &= \begin{cases} \overrightarrow{C_{i1}} + \left(s\tan\dfrac{\eta}{2}\right)\mathbf{m}_i, \ i = 1, \\ \overrightarrow{C_{i2}} + \left(s\tan\dfrac{\eta}{2}\right)\mathbf{n}_i, \ i = 2, \end{cases} \\
\overrightarrow{C_{i4}} &= \overrightarrow{C_{i1}} - \frac{s}{b_i}\left(\overrightarrow{B_i} - \overrightarrow{C_i}\right), \\
\overrightarrow{C_{i5}} &= \overrightarrow{C_{i1}} + r_i \frac{\overrightarrow{C_{i1}} + \overrightarrow{C_{i2}} - 2\overrightarrow{C_i}}{\|\overrightarrow{C_{i1}} + \overrightarrow{C_{i2}} - 2\overrightarrow{C_i}\|}, \\
\overrightarrow{C_{i6}} &= \overrightarrow{C_{i2}} - \frac{s}{c_i}\left(\overrightarrow{A_i} - \overrightarrow{C_i}\right),
\end{aligned}
\tag{24}
$$

for $i = 1$ and 2.

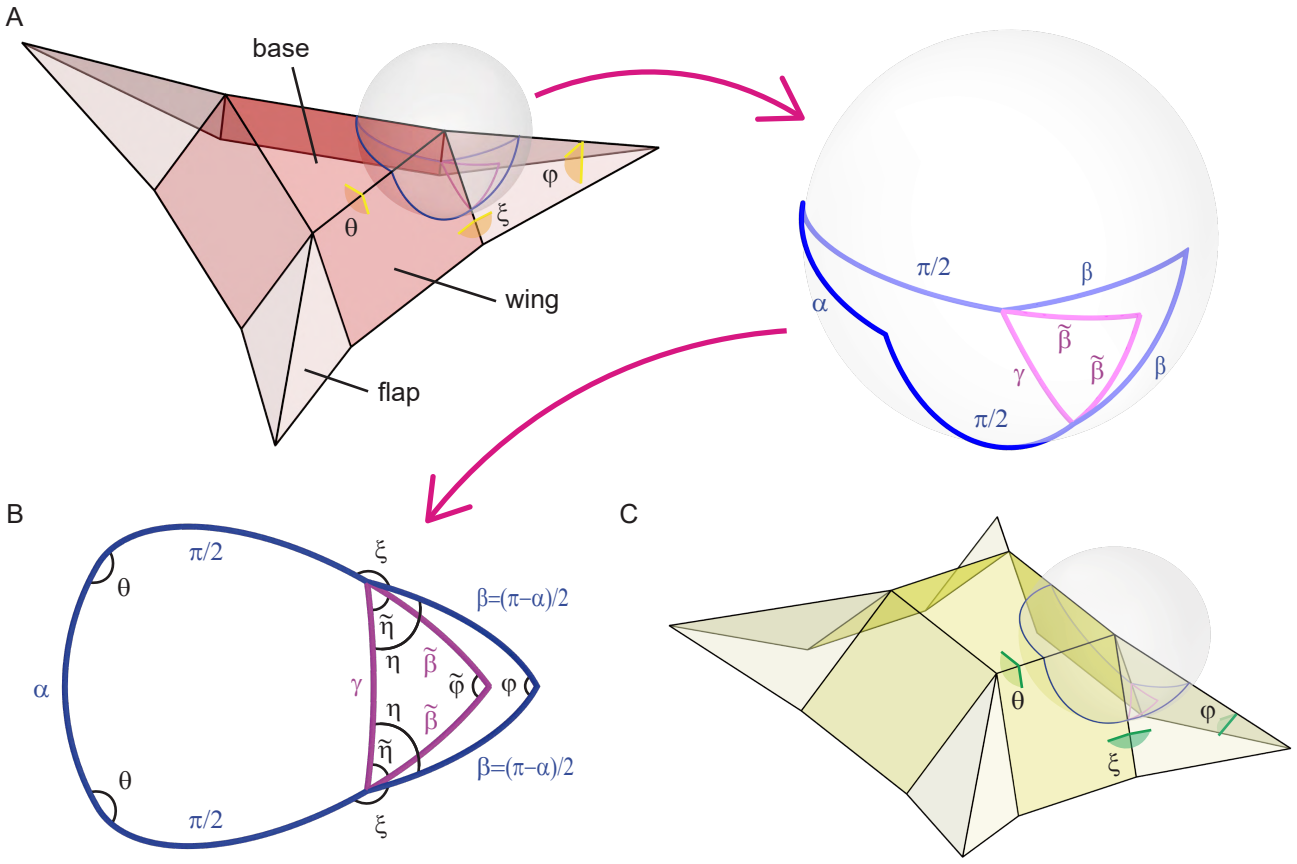

Fig. S1. Spherical geometry of unit cells of the folded kirigami. (*A*) The equilateral-triangular unit cell. (*B*) Geometric notations of the sector angles and dihedral angles. (*C*) The square unit cell.

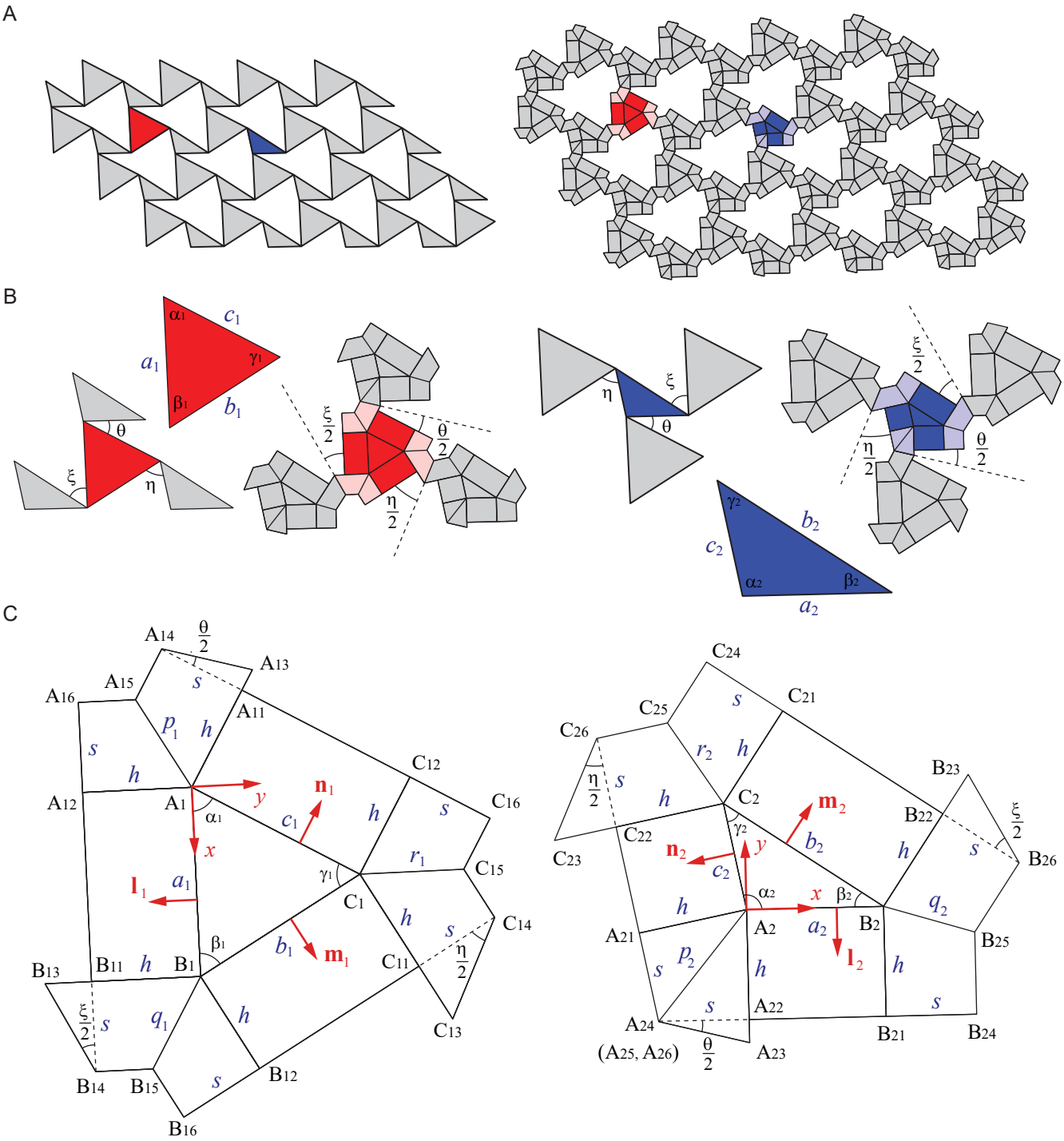

Fig. S2. Irregular kagome folded kirigami with two repeating constituent triangles. (*A*) Original kagome pattern (*Left*) and the corresponding crease-slit pattern for the folded kirigami (*Right*). (*B*) Two constituent triangles in the original pattern and the crease-slit pattern, respectively. (*C*) Repeating patches in the crease-slit pattern.

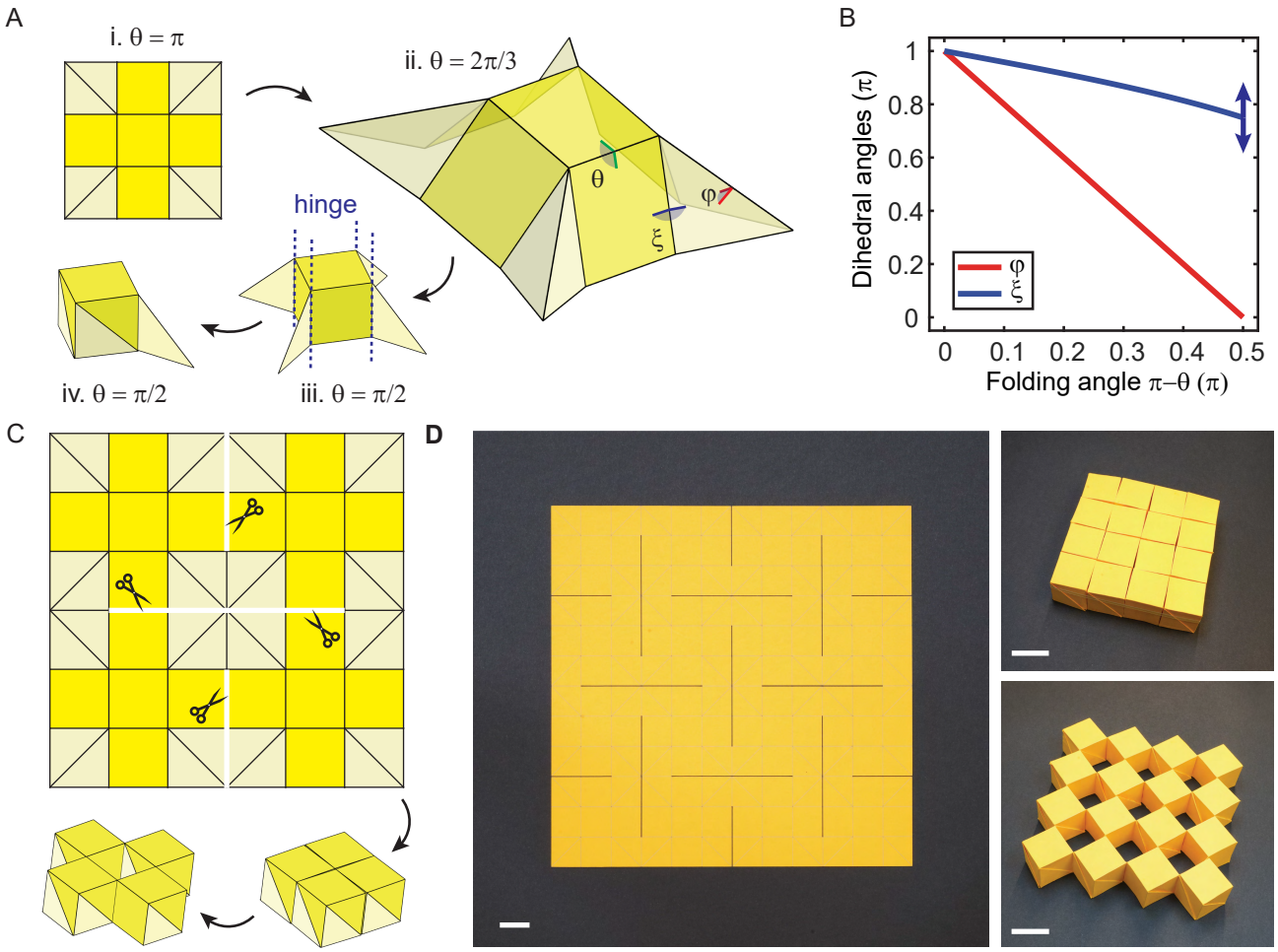

Fig. S3. Rotating-square folded kirigami. (*A*) Crease pattern for a square prism and its folding sequence. (*B*) Variation curves of dihedral angles. (*C*) Crease-slit pattern and its folded configurations of the rotating-square folded kirigami with a single loop. (*D*) Unfolded paper sheet with perforated cuts and engraved creases (*Left*) and its folded configurations (*Right*) of the rotating-square folded kirigami with multiple loops. (Scale bars, 3 cm.)

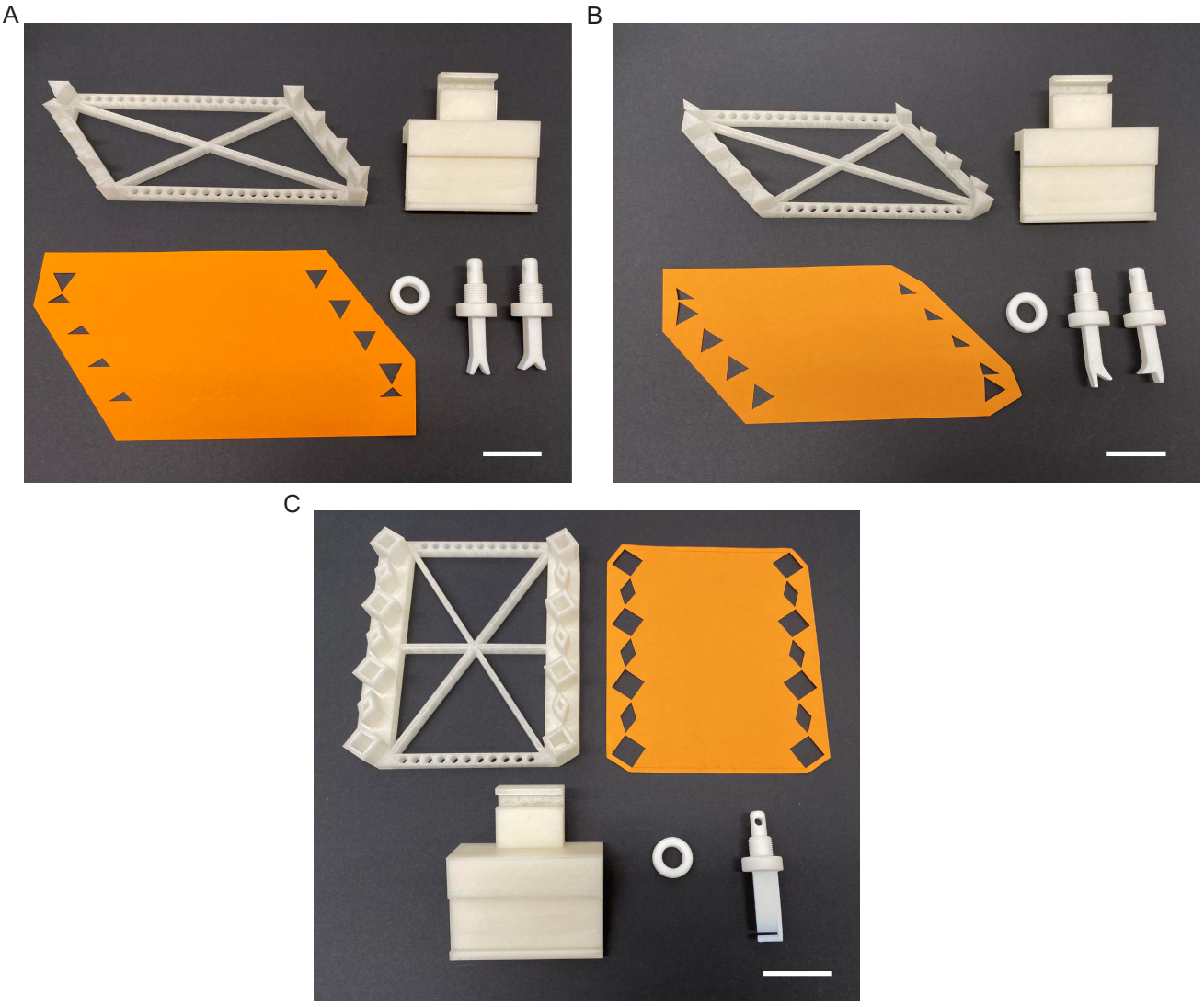

Fig. S4. Home-made experimental appliances for (*A*) the compression tests of the polarized configuration of the irregular kagome folded kirigami, (*B*) the compression tests of the non-polarized configuration of the irregular kagome folded kirigami, and (*C*) the compression and tension tests of the square-rhombus folded kirigami. (Scale bars, 5 cm.)

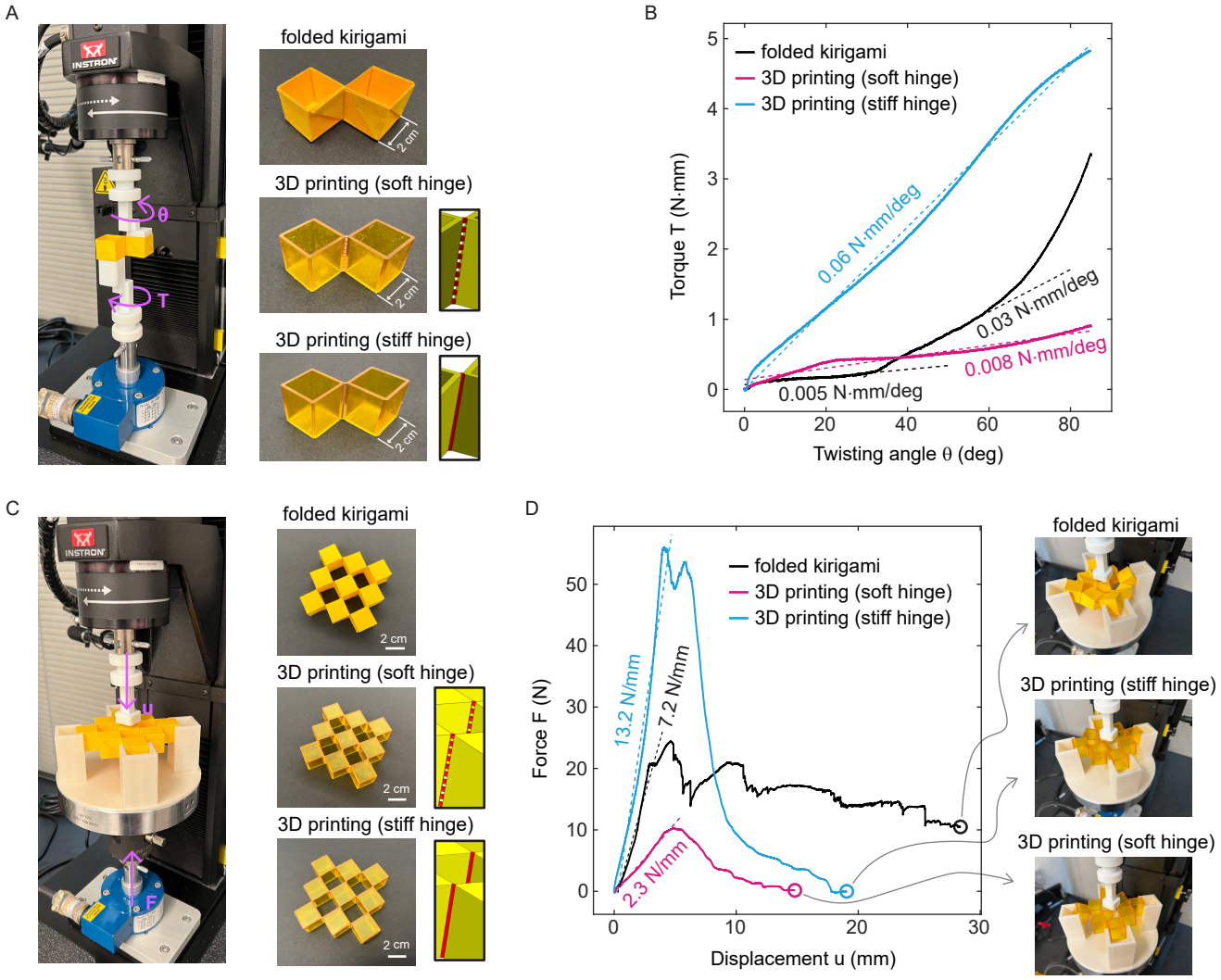

Fig. S5. Quasi-static twisting and bending tests for rotating squares made by "folded kirigami" and 3D printing approaches. (A) Experimental setup for the twisting (in-plane rotation) tests. (B) Experimental curves of torque T versus twisting angle θ. (C) Experimental setup for the bending (out-of-plane compression) tests. (D) Experimental curves of force F versus displacement u. The insets show the end of the experiments. Notice that the 3D printed configurations display zero force at the end of the experiment (red and blue circles) while the folded kirigami still displays a finite reaction force (the black circle). The latter test stops at the black circle because of the contact between the prototype and the bottom surface). The dashed lines in (B) and (D) represent linear regression of the experimental data. The folded kirigami is made of craft paper (Canson Colorline, 150 g/m^2). The 3D printed prototypes are made of Vero photopolymers for the cubes, and digital materials (mixed Vero and Elastico photopolymers, Shore-A 50) for the hinges. We used the 3D printer Stratasys J55 Prime. The stiff hinge is a cuboid of size $1\times1\times20$ mm^3. The soft hinge is an array of ten tiny cubes of size $1\times1\times1$ mm^3 each. The loading rate is 1 deg/s for the twisting test and 5 mm/min for the bending test.

Table S1. Area shrinkage from the flat pattern to the stereoscopic folded kirigami

Pattern	Area shrinkage
1. Regular kagome	88.9%
2. Rotating-square	88.9%
3. Irregular kagome	89.9%
4. Square-rhombus	83.8%

Movie S1. Deployment of regular kagome "folded kirigami"

Movie S2. Crease-slit patterns for kagome "folded kirigami"

Movie S3. Deployment of rotating-square "folded kirigami"

Movie S4. Compression tests of polarized & non-polarized kagome "folded kirigami"

Movie S5. Mechanical testing of non-reciprocal square-rhombus "folded kirigami"